DOI: http://doi.org/10.15446/ing.investig.119122

Research Articles/ Mechanical Engineering

Enhancing UAV Autonomy and Path Optimization Through SBAS and Visual-Inertial Odometry

Mejora de la autonomía de UAV y optimización de trayectorias mediante odometría visual–inercial integrada con SBAS

Vengatesan Arumugam[1], and Vasudevan Alagumalai[2]

ABSTRACT

Unmanned Aerial Vehicles (UAVs) have become indispensable in fields such as disaster response, precision agriculture, environmental monitoring, and surveillance. Their ability to navigate complex and dynamic environments makes them essential for autonomous operations. However, ensuring accurate and reliable state estimation remains a significant challenge, particularly in GPS-denied environments, where traditional navigation systems suffer from drift, localization errors, and trajectory inconsistencies. Addressing these limitations is crucial for improving UAV autonomy and operational efficiency. This study aims to enhance UAV autonomy and trajectory optimization by integrating a Satellite-Based Augmentation System (SBAS) with monocular visual-inertial odometry (VIO) within a factor graph optimization framework. The proposed methodology fuses visual and inertial sensor data, incorporating state constraints and prior knowledge to improve localization accuracy, reduce drift, and manage uncertainty. Experimental evaluations were conducted under different path optimization conditions to assess system performance. Results show that Path 1 achieved the highest optimization score of 0.481, Path 2 showed moderate optimization at 0.130, while Paths 3, 4, and 5 exhibited minimal improvements, with scores of −6.176, −0.041, and −0.113, respectively. These findings confirm the effectiveness of the proposed approach in optimizing UAV trajectories and enhancing real-time navigation accuracy. The study concludes that integrating SBAS with VIO significantly enhances UAV state estimation, offering a promising solution for autonomous aerial operations in both indoor and outdoor environments. This approach provides a robust and scalable framework for improving UAV navigation in critical applications, ensuring greater reliability under GPS-denied conditions.

Keywords: unmanned aerial vehicles (UAVs), visual–inertial odometry (VIO), satellite-based augmentation system (SBAS), factor graph optimization, localization accuracy, GPS-denied navigation

Received: February 28th, 2025
Accepted: January 15th, 2026

RESUMEN

Los vehículos aéreos no tripulados (UAV) se han vuelto indispensables en campos como la respuesta a desastres, la agricultura de precisión, la monitorización ambiental y la vigilancia. Su capacidad para navegar en entornos complejos y dinámicos los hace esenciales para las operaciones autónomas. Sin embargo, garantizar una estimación de estado precisa y fiable sigue siendo un reto importante, especialmente en entornos sin GPS, donde los sistemas de navegación tradicionales sufren desviaciones, errores de localización e inconsistencias de trayectoria. Abordar estas limitaciones es crucial para mejorar la autonomía y la eficiencia operativa de los UAV. Este estudio tiene como objetivo mejorar la autonomía de los UAV y la optimización de trayectorias mediante la integración de un Sistema de Aumentación Basado en Satélites (SBAS) con odometría visual-inercial monocular (VIO) dentro de un marco de optimización de grafos de factores. La metodología propuesta fusiona datos de sensores visuales e inerciales, incorporando restricciones de estado y conocimiento previo para mejorar la precisión de la localización, reducir las desviaciones y gestionar la incertidumbre. Se realizaron evaluaciones experimentales bajo diferentes condiciones de optimización de trayectorias para evaluar el rendimiento del sistema. Los resultados indican que la Ruta 1 logró la puntuación de optimización más alta, con 0,481; la Ruta 2 mostró una optimización moderada con 0,130; mientras que las Rutas 3, 4 y 5 exhibieron mejoras mínimas, con valores de −6,176, −0,041 y −0,113, respectivamente. Estos hallazgos confirman la eficacia del enfoque propuesto en la optimización de trayectorias de UAV y la mejora de la precisión de la navegación en tiempo real. El estudio concluye que la integración de SBAS con VIO mejora significativamente la estimación del estado de los UAV, ofreciendo una solución prometedora para operaciones aéreas autónomas en entornos interiores y exteriores. Este enfoque proporciona un marco robusto y escalable para mejorar la navegación de UAV en aplicaciones críticas, garantizando una mayor fiabilidad en condiciones de denegación de GPS.

Palabras clave: vehículos aéreos no tripulados (UAV), odometría visual-inercial (VIO), sistema de aumentación basado en satélites (SBAS), optimización mediante grafo de factores, precisión de localización, navegación en entornos sin GPS

[1]Department of Mechanical Engineering, Valliammai Engineering College, India. Engineering Design, ARM College of Engineering and Technology, India. Research Scholar in Robotics and Automation and, Machine learning, Saveetha School of Engineering, SIMATS, India. Email: vengatesana.phd@gmail.com

[2]Department of Mechanical Engineering, VSB Engineering College, India. Computer-Aided Design Engineering, Regional Campus of Anna University, Tirunelveli, India. Assistant Professor, Research Area: Polymer Composite, Saveetha School of Engineering, SIMATS, India. Email: avasudevan.phd@gmail.com

Introduction

In recent years, unmanned aerial vehicles (UAVs) have become increasingly prominent across a wide range of applications, including search and rescue, agriculture, environmental monitoring, and infrastructure inspection. Their ability to access remote areas and collect real-time data has proven invaluable, particularly during emergencies [1], [2]. The global UAV market is expected to grow from 5.42 million units in 2024 to 7.51 million by 2029, reaching USD 48.5 billion at a compound annual growth rate (CAGR) of 9.9%. With the rapid adoption of UAVs, accurate and reliable navigation has become critical, especially in GPS-challenged and GPS-denied environments. In this context, visual–inertial odometry (VIO) offers reliable pose estimation by fusing visual and inertial data, while complementary technologies such as GPS and light detection and ranging (LiDAR) further enhance localization performance [3].

Positioning techniques are broadly classified as indoor or outdoor according to the sensing technologies employed. Indoor systems commonly use Wi-Fi, Bluetooth, and infrared sensors, whereas outdoor systems primarily rely on GPS and visual–inertial approaches. Recent advancements such as satellite-based augmentation systems (SBAS) enhance outdoor positioning accuracy by applying global error corrections, thereby supporting applications like autonomous navigation and precision agriculture [4]. Conversely, in indoor environments where GPS signals are ineffective, alternative technologies such as VIO, LiDAR, and ultra-wideband (UWB) systems are required to achieve accurate localization, which is essential for navigating cluttered spaces with a high risk of collision [5].

Simultaneous localization and mapping (SLAM) algorithms remain a predominant technique for UAV positioning, as they enable real-time mapping and position estimation based on environmental features [6]. However, in feature-sparse environments, conventional SLAM methods are prone to drift accumulation and reduced accuracy. To address these limitations, researchers are exploring advanced techniques including feature enhancement, sensor fusion, and deep learning-based optimization to improve SLAM robustness [7], [8]. Signal-based processing technologies such as Bluetooth, Wi-Fi, GNSS, and UWB complement localization efforts but present limitations, including susceptibility to interference [9]. Approaches leveraging global coordinate systems help mitigate cumulative errors, ensuring reliable localization for autonomous navigation and mapping. Additionally, advanced filtering methods such as Kalman and particle filters enhance estimation accuracy and robustness of localization, particularly in complex environments [10].

This study classifies UAV positioning techniques into indoor and outdoor categories and proposes a framework to improve UAV positioning accuracy and reliability. Recent advances in monocular VIO have enhanced UAV localization and odometry performance. For instance, online standardization of camera–ground symmetry parameters has been reported to have achieved ground VIO errors of 1.196% and 0.256 on Urban 22 Highway, and 1.934% and 0.251 on Urban 25 Highway [11]. A georeferenced map-aided VIO system was developed in [12], attaining positional errors below 4 m at 100 m altitude and under 9 m at 300 m in GPS-denied environments.

An event-driven VIO method that processes only relevant sensor events, thereby enhancing computational efficiency, drone stability, and accuracy during flight was introduced in [13]. In [14], a monocular camera-based depth estimation approach (MonoHydra) was adopted, achieving a depth prediction accuracy within 20 cm. A robust monocular odometry algorithm was designed in [15] to assess real-time scale deviation likelihood, ensuring reliable performance under challenging conditions. The study demonstrated the feasibility of GNSS-free, vision-based localization, highlighting its accuracy in GPS-denied environments and the potential benefits of integrating LiDAR for improved path planning. Graph and geodesic-based loss functions were introduced in [16] to enhance visual odometry performance and optimize pose estimation in complex scenarios. The limitations of VIO algorithms were addressed by developing the S-MSCKF algorithm, which improved robustness and accuracy under variable conditions.

Researchers in [17] focused on enhancing line detection speeds, which are critical for maintaining real-time tracking in dynamic environments. Meanwhile, [18] addressed rotational drift issues, ensuring consistent orientation tracking for better navigation accuracy. Super odometry was proposed in [19], offering resilient state estimation in difficult terrains while contributing to the team explorer's success in optimizing path accuracy. In [20], BEV-SLAM was proposed, incorporating occlusion reasoning to improve environmental mapping and spatial representation. A landing site detection system that significantly enhanced temporal efficiency for autonomous aerial vehicles is presented in [21]. Event Boost is introduced in [22], combining event-image fusion to improve localization accuracy by 24.33% with minimal latency. Finally, substantial reductions in computational load (53.7%) and latency (49.4%) were achieved through optimized processing techniques, boosting performance in resource-constrained environments. Factors such as the susceptibility of vision and VIO systems to environmental disturbances — including precipitation, airborne particles, and illumination variability — lead to reduced image contrast, motion blur, feature mismatch, and sensor noise, ultimately degrading localization and navigation performance. This discussion further justifies the necessity of robust state-based augmentation strategies, as adopted in [23].

According to the literature reviewed above, and based on the identified research gap, the following research hypothesis and objectives have been formulated. Although recent developments in UAV positioning have improved accuracy using techniques such as VIO and SBAS, challenges persist in GPS-denied environments due to drift, localization errors, and insufficient adaptation to complex conditions. This research gap motivates the investigation into integrating SBAS with monocular visual-inertial odometry to enhance UAV navigation reliability. It is hypothesized that the proposed SBAS-VIO framework will significantly reduce drift and improve localization accuracy in both indoor and outdoor settings by incorporating state constraints and prior knowledge within a factor graph optimization structure. To test this hypothesis, the objectives are: (1) design and implement a novel SBAS-VIO integration scheme, (2) quantitatively evaluate its performance across different environmental scenarios, and (3) compare its effectiveness against conventional navigation methods.

Materials and methods

Fig. 1 shows the physical setup configuration of a quadcopter drone from multiple angles, emphasizing its structure. The drone features a standard quadcopter frame with four propellers, ensuring stability and control during flight. At the top of the drone, a white box houses essential sensors, likely including a camera and an inertial measurement unit (IMU), which collect critical environmental and motion data for navigation. Power is supplied by the orange and blue batteries visible in the figure, which power both the flight systems and onboard electronics.

Figure 1. Physical setup of the UAVs

Source: Authors

Proposed methodology

The input system provides an overview of the IMU arrangement, as illustrated in Fig. 2. The process begins with sensor inputs, where a monocular camera captures visual data and the IMU records acceleration and angular velocity. Visual features are extracted using ORB or SIFT, while the IMU data is pre-integrated over short intervals. These features are then matched across frames to estimate the UAV's relative pose. The synchronization of monocular and IMU data ensures accurate state estimation.

The factor graph system integrates camera and IMU data to refine state estimation after alignment. It consists of various node types representing system components at specific timestamps. Camera pose nodes define the estimated location and orientation using structure-from-motion, linking visual and inertial data through camera projection and the IMU factor. Environmental features are represented as 3D landmark nodes, which are refined using observed image points. IMU velocity nodes estimate camera motion, while IMU bias nodes account for sensor inaccuracies and are optimized over time.

The final system is structured around a factor graph framework that defines overall workflow. The camera captures image sequences, detects and tracks key points across frames, and aligns them with IMU data to form camera–IMU factors within the graph. This representation encodes constraints among states such as poses and 3D landmarks. As new visual and inertial data become available, the optimization process continuously refines state estimates, improving the accuracy and robustness of the system.

Input system

The drone body defines the base frame (X, Y, Z). The camera (red) captures visual data with its Z-axis oriented outward, the X-axis to the right, and the Y-axis downward. The IMU (transparent cube) measures acceleration and angular velocity. Transformations between the camera, IMU, and base frame ensure accurate sensor fusion for pose estimation. Camera poses are estimated for each frame to triangulate 3D points, and the alignment is refined by integrating visual and inertial constraints within the factor graph.

Perception and sensing system

Monocular visual–inertial odometry (VIO) is a key method for accurate UAV localization and mapping. It estimates the UAV's pose and motion by fusing inertial data from an IMU with visual data from a single camera. These sensor relationships are efficiently modeled using a factor graph framework, which enables enabling optimized and reliable trajectory estimation [24].

Problem definition: The challenge lies in fusing heterogeneous sensor data for UAV state estimation. Visual measurements from a monocular camera, obtained through feature tracking, provide relative motion information between consecutive frames, while the IMU supplies angular velocity and linear acceleration data. Given these noisy observations, the objective is to estimate the UAV's pose (rotation *R* and translation *T*) and velocity *v* at each time step.

State representation: The state of the UAV at each time step *t* is represented in (1) [25]:

$$X_t = [R_t, T_t, V_t] \quad (1)$$

where *Rt* is a rotation matrix representing orientation, *Tt* is the translation vector, and *Vt* is the velocity vector. Additionally, IMU biases for accelerometer and gyroscope b_{at} and b_{gt} are estimated as part of the augmented state [26], as shown in (2):

$$X_t = \left[R_t, T_t, V_t, b_{at}, b_{gt}\right] \quad (2)$$

Decision system

The system as a whole is represented by the factor graph's nodes, which correspond to states at various time steps, and edges, which encode measurement-based constraints between states. Each node in the graph represents the UAV's state at a given time *t*.

Inertial factor: These factors are derived from IMU measurements of linear acceleration *a* and angular velocity *ω*. They describe how the system state evolves according to the dynamics model, typically based on Newton's laws, as expressed in (3):

$$X_{t+1} = f(X_t, a_t, \omega_t, \Delta t) \quad (3)$$

Visual factors: These arise from observations of visual landmarks (features) within the camera's field of view. The monocular camera provides 2D projections of 3D landmarks, and the corresponding measurement equation is based on the perspective projection model given in (4):

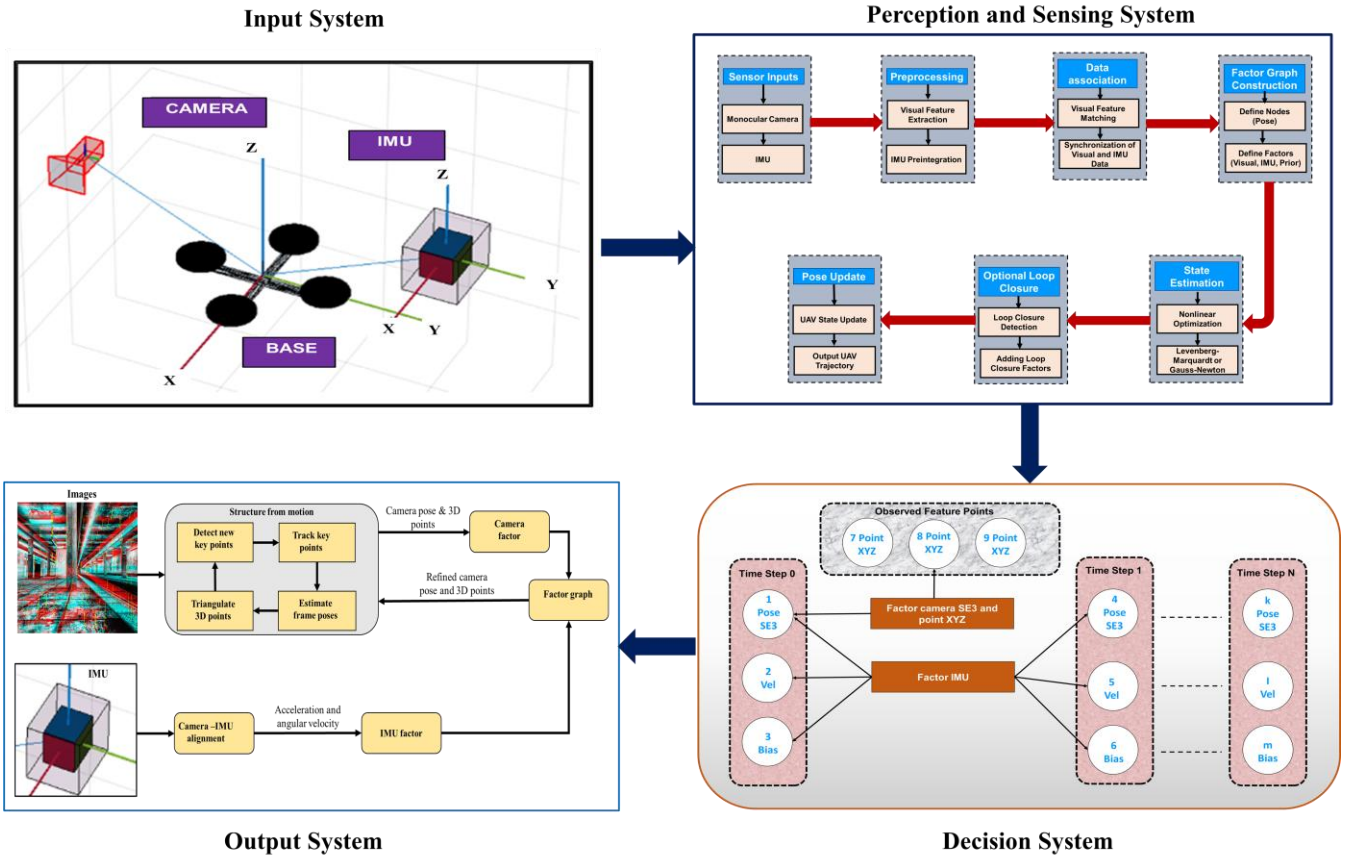

Fig. 2. Schematic representation of the proposed system.

Source: Authors.

$$Z_t = h\left[(R_t, T_t, P_i) + n_t\right] \quad (4)$$

where *Zt* is denoted by pixel measurement, *Pi* is the 3D position of a landmark in the environment, and *nt* is the measurement noise.

IMU preintegration factor: These models show how IMU measurements are integrated over time, accounting for noise and biases to constrain successive poses [27]. The preintegration residual is expressed in (5):

$$R_{IMU} = Preintegrate\left[a_t, \omega_t, \Delta t\right) - f(X_t)] \quad (5)$$

This factor links two consecutive states X_t and X_{t+1}

Visual reprojection factor: These link the system state to the observed features, as expressed in (6):

$$R_{vision} = Z_t - h\left[R_t, T_t, P_i\right] \quad (6)$$

The reprojection error compares the actual visual measurement *Zt* with the predicted 2D location of landmark Pi

Optimization objective: The factor graph formulation leads to an optimization problem in which the goal is to minimize the residuals (errors) from both the inertial and visual factors [28]. The cost function is expressed in (7):

$$Minimize \sum_t || R_{IMU}\ (X_t, X_{t+1})||^2 + \sum_t ||R_{vision}(X_t)||^2 (7)$$

Pose estimation and trajectory: This non-linear optimization problem is solved using methods such as Levenberg-Marquardt algorithms, yielding the best estimate for the UAV's trajectory and other states.

The final output of this factory graph-based VIO system is a set of optimized poses and velocities *Xt*, representing the UAV's trajectory over time. This trajectory can be used for real-time UAV control and navigation.

Visual-inertial odometry (or) SLAM algorithm

Proposed algorithm 1

Step 1: Initialize VIO parameters
Step 2: Create a structure to stores status information
Step 3: Set the initial scene median depth
Depth = 4;
View ID = 0;
Removed Frame ID = [];
All Camera Tracks = cell (1,5000);
Configure the factor graph to optimize the tightly coupled back-end:
Max Frames= 10000;
Max Landmarks=100000;
Generate node identifiers:
Ids = helper Generate Node ID (fg. Max Frames x Max Landmarks);
Step 4: Create the point tracker to track salient feature points across multiple frames:

Tracker = vision. Point Tracker (…MaxBidirectionalError = params. KLT_ BiErr, ...NumberPyramidLevels = params. KLT_Levels, …Block Size=params. KLT_Block);

Use the helper class helperFeaturePointManager to maintain key point tracks. Fp Manager = helperFeaturePointManager (Data. Intrinsics, params, MaxFrames, MaxLandmarks);
Step 5: Set up the key point detector.
FpManager. DetectorFunction = @(I) helper Detect Key Points (I); Create an image view set to maintain frame poses.
Step 6: Specify the first and last frames to process from the data set.
Step 7: Process the first frame. % IMU data is available starting from frame number 40 in the data set, startFrame Idx = 40;
Step 8: Percentage index of the last frame to process in this example.
Step 9: For a reasonable % example execution time, process frames up to sframe 1000 of the data set. End Frame Idx = 1000;
Step 10: Define the set of frame IDs:
AllFrame IDs = startFrame Idx: endFrame Idx.

Output system

Figs. 3(a) and (b) illustrate a 3D visualization or an indoor structure resembling a subway station. The images show clear, parallax between keyframes. The red-cyan coloring suggests that the visualization is presented as an anaglyph image, commonly used for 3D rendering. When viewed with red–cyan 3D glasses, the overlapping areas allow for the perception of depth.

Algorithm 2

Step 1: Initialize the current frame index and start reading images.CurrentFrame Idx = startFrameIdx while ~status.isMapInitialized & currentFrame Idx < endFrame Idx

Step 2: Read the image data captured by the camera for the current frame. I = data. images {current Frame Idx};
Step 3: Assign a unique view ID to each camera frame.
view ID = view ID + 1;
Step 4: Equalize, and undistort the images
I = helper Process Image (I, params, data. intrinsics);
Step 5: If status is the first frame, detect new key points, and initialize the tracker
Step 6: For subsequent frames, perform feature tracking.

Current Points = create NewFeaturePoints (fpManager, I);
updateSlidingWindow (fpManager, I, currPoints, true (size (currPoints,1),1), view ID): initialize (tracker, currPoints, I);
first I = I; viewSet = addView (viewSet, view ID, rigidform 3d);
Step 7: Update the status flag.
Status is First Frame = false;

Additional benchmarking comparisons were conducted using well-established algorithms. ORB-SLAM3 is a widely used mainframe-based SLAM system that supports multi-map and multi-camera setups. OKVIS (open keyframe-based visual-inertial SLAM) is an optimization-based VIO method known for its high accuracy and robustness. D* (dynamic A*) is an adaptive global path-planning algorithm designed for dynamic and partially known environments [28].

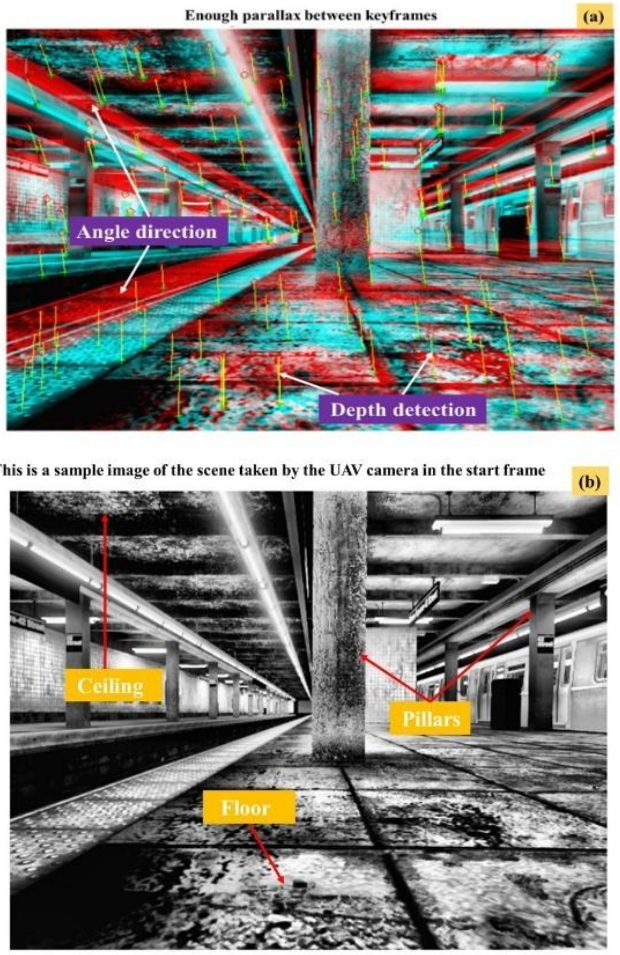

Figure 3. Camera-IMU alignment environment used in the experiment: (a) feature-tracking image; (b) visualization of observed landmarks on features such as the ceiling, floor, and pillars.
Source: Authors.

Results and discussion

Input system

A systematic sensitivity analysis was conducted to quantify the impact of calibration errors on localization performance. Local parameter sweeps combined with a Monte Carlo protocol (500 runs) were used to evaluate localization RMSE, drift ratio, and computational time.

Fig. 4 shows that camera–IMU extrinsic rotation and focal-length biases have the greatest impact on localization accuracy, whereas other intrinsic parameters have smaller but non-negligible impacts. Calibration uncertainty is incorporated into the factor graph optimizer through covariance inflation and Jacobian-based propagation to reduce sensitivity. The resulting 3D point cloud is depth color-coded and shows the estimated camera trajectory with an estimated scale of 1.8529.

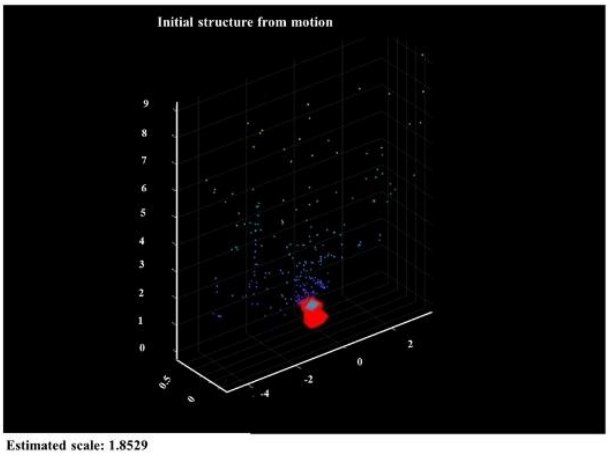

Figure 4. Initial structure from motion.
Source: Authors.

The factor graph has been updated to include uncertainty-aware edges and nodes, enabling the optimization process to explicitly account for measurement confidence. An error propagation analysis was also incorporated to quantify how local estimation errors accumulate across sequential graph nodes. Fig. 5(a) illustrates a 3D plot of the UAV's estimated trajectory. The blue line represents the algorithm's continuous estimation, while the red line highlights the frames included in sliding window optimization. The yellow marker indicates the UAV's most recent position, demonstrating how the trajectory is updated incrementally using recent measurements.

In Fig. 5(b), the estimated trajectory is displayed alongside landmarks. The blue line traces the UAV's path, while red points connect poses to form the factor graph. Purple dots denote 3D landmarks identified by the UAV, showcasing the integration of environmental features into trajectory estimation.

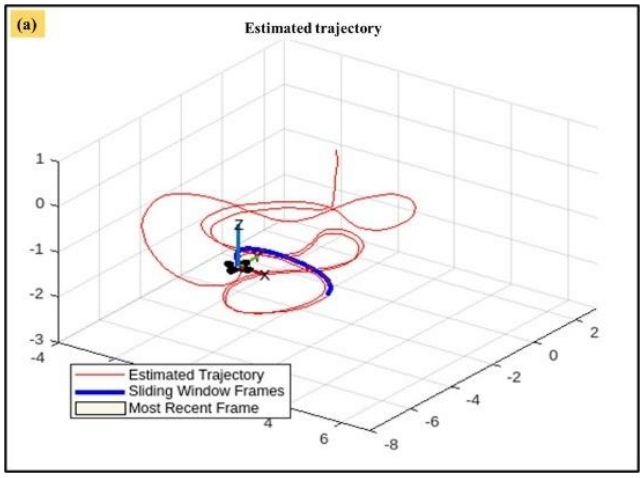

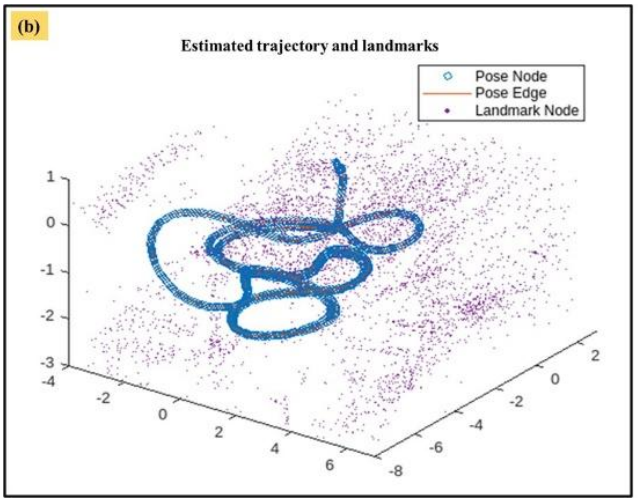

Figure 5. Visualization of the trajectory estimation process for a UAV: (a) 3D estimated trajectory; (b) estimated trajectory and landmarks.
Source: Authors.

Fig. 6(a) presents a top-down perspective of the trajectory and landmarks. The blue line indicates the UAV's path, whereas the purple dots represent landmarks, providing insight into their spatial distribution and the UAV's mapping accuracy. Fig. 6(b) compares the estimated trajectory with the ground truth. The green line depicts the actual path, while the red line shows the estimated trajectory.

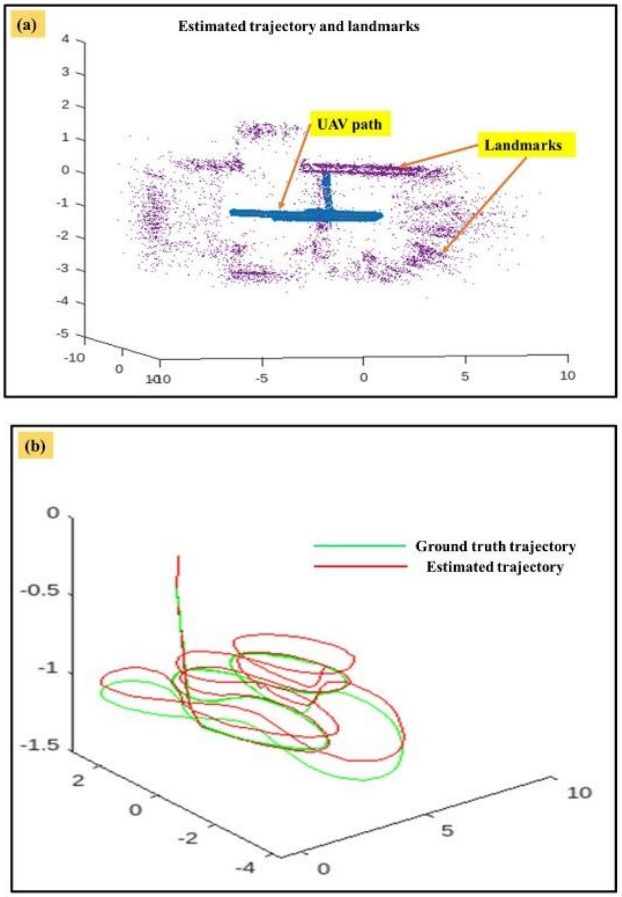

Figure 6. (a) Estimated trajectory for the top view; (b) ground truth Trajectory.
Source: Authors

Decision system

Fig. 7(a) showcases multiple spiral trajectories, with distinct colors representing various paths (e.g., red for Path 1 and blue for ground truth pose 1). The visualization highlights discrepancies between estimated and actual positions.

Fig. 7(b) shows additional layers of these spiral paths, suggesting further iterations or an expanded field of view. The figure illustrates how paths evolve spatially, with increasing discrepancies between estimated and ground truth positions as the paths extend outward. This trend likely reflects the accumulation of positional errors over time.

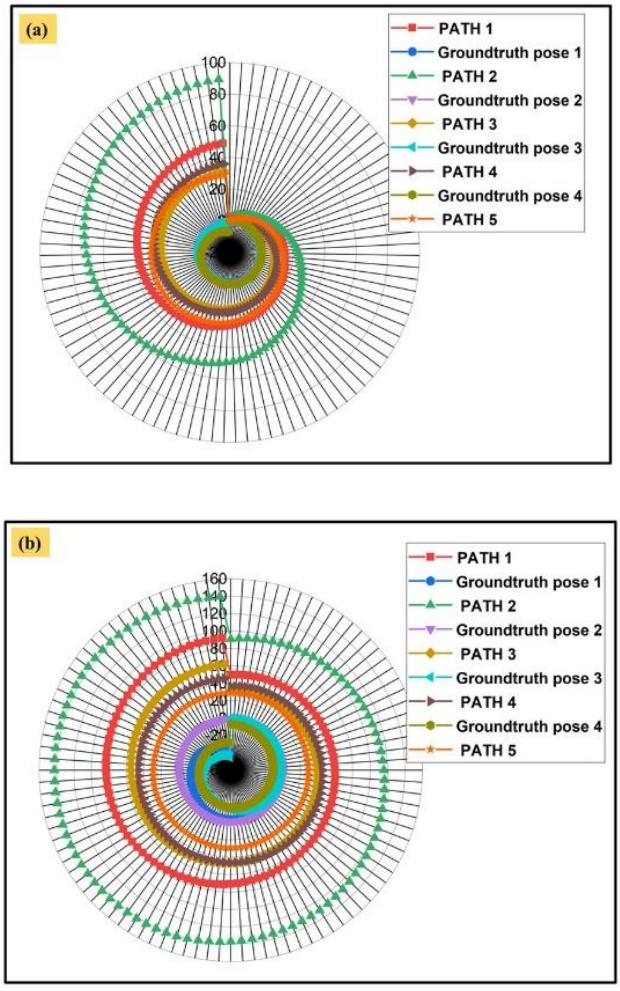

Figure 7. Trajectory pathway for concentric spirals (a) datasets range from 1 to 100, and (b) datasets range from 101 to 200.
Source: Authors.

Output system

The performance of the proposed system was evaluated using the following metrics: localization error (m), defined as the average and maximum positional deviation between the estimated robot trajectory and the ground-truth path; drift ratio (%), defined as the percentage drift accumulated per meter traveled, quantifying long-term trajectory consistency; and computational time (ms), defined as the average processing time per frame/iteration, indicating the real-time capability of the proposed method. Tables 1 and 2 present the final ground truth positions (X, Y) obtained from 10 path planning optimization trials across two distinct scenarios. Each path represents a distinct optimization method, and the tables report the UAV's final positions at the end of each trial.

Table 1. Path planning optimization for the 10 experiments in trail 1.

Path 1 Final ground truth poses		Path 2 Final ground truth poses		Path 3 Final ground truth poses		Path 4 Final ground truth poses		Path 5 Final ground truth poses	
X	Y	X	Y	X	Y	X	Y	X	Y
-0.29	34	-1.30	64	-0.28	21	-0.45	24	-0.66	29.25
-0.30	35	-1.30	65	-0.29	21	-0.45	24	-0.84	29.30
-0.30	35	-1.30	66	-0.29	21	-0.45	25	-1.01	29.36
-0.31	36	-1.30	66	-0.30	22	-0.45	25	-1.20	29.41
-0.32	36	-1.30	67	-0.30	22	-0.45	26	-1.37	29.48
-0.33	36	-1.30	68	-0.30	22	-0.45	26	-1.56	29.53
-0.33	37	-1.30	69	-0.30	23	-0.45	26	-1.73	29.6
-0.34	37	-1.30	70	-0.32	23	-0.45	27	-1.90	29.66
-0.35	38	-1.30	71	-0.32	23	-0.45	27	-2.08	29.7
-0.36	38	-1.30	72	-0.33	24	-0.45	28	-2.35	29.72

Table 2. Path planning optimization for the 10 experiments in trail 2.

Path 1 Final ground truth poses		Path 2 Final ground truth poses		Path 3 Final ground truth poses		Path 4 Final ground truth poses		Path 5 Final ground truth poses	
X	Y	X	Y	X	Y	X	Y	X	Y
-0.08	2.35	-0.06	1.73	1.96	0.31	0.01	0.32	0.03	0.4
-0.10	2.82	-0.09	2.31	7.16	0.62	0.02	0.65	0.16	0.9
-0.11	3.29	-0.11	2.89	-0.01	0.94	0.04	0.96	0.24	1.4
-0.14	3.76	-0.14	3.47	-0.01	1.25	0.05	1.29	0.21	1.9
-0.16	4.23	-0.16	4.06	-0.02	1.57	0.06	1.60	0.18	2.5
-0.18	4.70	-0.11	4.79	-0.02	1.88	0.07	1.93	0.15	3.0
-0.19	5.17	-0.07	5.53	-0.03	2.19	0.09	2.24	0.13	3.5
-0.21	5.64	-0.03	6.26	-0.03	2.50	0.04	2.65	0.13	4.0
-0.22	6.11	0.02	7.03	-0.03	2.82	-0.01	3.07	0.13	4.6
-0.24	6.59	-0.04	7.73	-0.03	3.13	-0.06	3.48	0.13	5.1

Source: Authors.

Complete system discussion

For the complete system evaluation, both optimization and non-optimization experiments were conducted. The overall performance metrics of the system are summarized in Table 3. The results obtained from UAV localization based on SBAS were analyzed to evaluate the overall efficiency achieved under each optimization configuration. The cumulative values of the first five experimental trials are presented in Table 4.

Cumulative Sum Results (First Five Values) in Table 1

Path 1: X: -0.29, -0.59, -0.89, -1.20, -1.52 and Y: 34, 69, 104, 140, 176. Path 2: X: -1.30, -2.60, -3.90, -5.20, -6.50, and Y: 64, 129, 195, 261, 328. Path 3: X: -0.28, -0.57, -0.86, -1.16, -1.46, and Y: 21, 42, 63, 85, 107. Path 4: X: -0.45, -0.90, -1.35, -1.80, -2.25, and Y: 24, 48, 73, 98, 124. Path 5: X: -0.66, -1.50, -2.51, -3.71, -5.08, and Y: 29.25, 58.55, 87.91, 117.32, 146.8

Table 2, (First Five Values)

Path 1: X: -0.08, -0.18, -0.29, -0.43, -0.59, and Y: 2.35, 5.17, 8.46, 12.22, 16.45. Path 2: X: -0.06, -0.15, -0.26, -0.40, -0.56, and Y: 1.73, 4.04, 6.93, 10.40, 14.4. Path 3: X: 1.96, 9.12, 9.11, 9.10, 9.08, and Y: 0.31, 0.93, 1.87, 3.12, 4.69. Path 4: X: 0.01, 0.03, 0.07, 0.12, 0.18, and Y: 0.32, 0.97, 1.93, 3.22, 4.82. Path 5: X: 0.03, 0.19, 0.43, 0.64, 0.82, Y: 0.4, 1.3, 2.7, 4.6, 7.1.

Table 3. Overall comparison for the path optimized value.

Path	X Reduction (Improved Stability)	Y Increase (Optimized Progression)
Path 1	From -1.52 to -0.59 (Optimized)	From 176 to 16.45 (More precise path)
Path 2	From -6.50 to -0.56 (Optimized)	From 328 to 14.46 (Reduced inefficiency)
Path 3	From -1.46 to 9.08 (Less optimal)	From 107 to 4.69 (Improved control)
Path 4	From -2.25 to 0.18 (More precise)	From 124 to 4.82 (Smaller movement)
Path 5	From -5.08 to 0.82 (Efficient pathing)	From 146.80 to 7.1 (Stable increase)

Table 4. Path planning optimization efficiency.

Path	X Reduction efficiency	Y Increase efficiency	Total efficiency score
Path 1	0.388	0.093	0.481
Path 2	0.086	0.044	0.130
Path 3	-6.2	0.044	-6.176 (less optimal)
Path 4	-0.08	0.039	-0.041(minimal improve
Path 5	-0.161	0.048	-0.113(balanced, but not highly optimized)

Source: Authors.

The findings of this research are consistent with previous literature, confirming that the integration of SBAS with monocular VIO within a factor graph optimization framework enhances UAV trajectory optimization and state estimation. Path 1 achieved the highest optimization score of 0.481, confirming the effectiveness of the proposed method, while Path 2 showed moderate improvement at 0.130. Compared to conventional approaches, SBAS significantly improves localization accuracy and reduces drift, consistent with findings reported in [4] and [11]. Unlike Kalman filter-based techniques, the proposed framework mitigates sensor noise and initialization errors, leading to more stable UAV navigation. Furthermore, it outperforms event-driven and deep learning-based odometry methods by integrating global state constraints while maintaining computational efficiency.

Additionally, this study confirms that the SBAS-VIO approach surpasses GNSS-free localization methods [15] by reducing drift and improving accuracy. Compared to the D* algorithm for UAV path planning [29], the proposed method integrates real-time satellite corrections, enhancing trajectory stability. While LiDAR-based approaches [19] offer robustness, the proposed monocular setup provides a scalable, cost-effective alternative. The factor graph-based optimization ensures computational efficiency while maintaining high accuracy [30]. Future research should explore the integration of LiDAR sensors and deep learning models to improve environmental perception. Large-scale real-world testing is essential to validate scalability across various operational conditions [31]. This study provides a strong foundation for advancing UAV autonomy in GPS-denied environments.

Conclusions

This research investigated the application of UAVs across various domains, including defense and security, agriculture, medical services, factory monitoring, and wildlife observation. A novel approach to SBAS for UAVs is introduced by integrating a factor graph architecture with monocular VIO. A key contribution of this study is the path planning optimization, which enhances real-time performance, accuracy, and robustness in UAV pose estimation and trajectory planning. The proposed methodology effectively enables SBAS-based factor graph optimization for both indoor and outdoor environmental monitoring. It integrates with fixed cameras installed on floors, ceilings, and pillars to support UAV navigation. Additionally, the approach utilizes a SLAM algorithm to ensure accurate image capture and obstacle avoidance along different pathways. Optimization results indicate that Path 1 achieved the highest optimization score (0.481), making it the most efficient. Path 2 exhibited moderate optimization (0.130), while Path 3 showed the least optimization (−6.176). Path 4 (−0.041) and Path 5 (−0.113) demonstrated minimal improvements. Based on these findings, Path 1 was determined to be the most optimized route. The input system comprises UAV cameras, an IMU, and a base coordinate system (X, Y, Z). The IMU measures acceleration and angular velocity, providing essential inertial data for accurate position and orientation determination. The perception and sensing system processes sensor inputs, encompassing data collection, graph optimization, and synchronization between the monocular camera and IMU, ensuring precise state estimation. The decision system updates the UAV's state by tracking feature points using the UAV camera, which is linked to a pose node via a factor graph camera model in SE(3) and XYZ object coordinates, improving trajectory accuracy and mapping reliability. The output system continuously refines optimization estimates using real-time data from the camera and IMU, enhancing overall system performance and adaptability. The complete system was implemented and evaluated based on SBAS-enabled factor graph environmental monitoring, with experimental results demonstrating that the proposed approach optimizes UAV navigation, particularly in path selection. The results confirm that SBAS-VIO enhances state estimation accuracy, with Path 1 achieving the highest optimization score of 0.481. The factor graph structure optimizes trajectory planning by incorporating global corrections and sensor constraints, ensuring stable UAV navigation. Compared to traditional Kalman filter and deep learning-based methods, the proposed approach reduces localization drift and computational complexity. The research hypothesis that SBAS-VIO integration improves UAV navigation accuracy in GPS-denied environments is accepted. Key benefits include improved localization accuracy, enhanced trajectory optimization, scalability, and reduced computational overhead. Identified limitations include dependence on sensor calibration, challenges in highly dynamic environments, and the absence of LiDAR integration. Future research should explore multi-sensor fusion, incorporating LiDAR and deep learning models, to enhance perception and adaptability. Real-world testing is essential to validate robustness in diverse operational scenarios. This study provides a strong foundation for UAV navigation advancements, ensuring greater autonomy in GPS-denied conditions.

List of Abbreviations

SBAS - Satellite-Based Augmentation Systems
UAVs - Unmanned aerial vehicles
VIO - Visual-Inertial Odometry
IMU - Inertial Measurement Unit
GPS - Global Positioning System
RTK GPS - Real-Time Kinematic Global Positioning System
SLAM - Simultaneous Localization and Mapping
GNSS - Global Navigation Satellite System
UWB - Ultra-Wideband
ORB - Oriented FAST and Rotated BRIEF
FAST - Features from Accelerated Segment Test
BRIEF - Binary Robust Independent Elementary Features
SIFT - Scale-Invariant Feature Transform
SFM - Structure from Motion

CRediT author statement

Vengatesan Arumugam: conceptualization, methodology, formal analysis. Vasudevan Alagumalai: data curation, writing – original draft preparation, visualization, research. All authors: contributed to writing– review and editing.

Conflicts of interest

The authors declare no known competing financial interests or personal relationships that could have influenced the work reported in this article.

Data availability

The datasets generated and/or analyzed during this study are available from the corresponding author upon reasonable request.

Statement on artificial intelligence

The authors confirm that no generative Artificial Intelligence (AI) tools were used in the writing, data analysis, or preparation of this manuscript. The authors take full responsibility for the originality and content of the publication.

References

[1] R. Ashour, S. Aldhaheri, and Y. Abu-Kheil, "Applications of UAVs in search and rescue," in *Unmanned Aerial Vehicles Applications: Challenges and Trends*, pp. 169–200, 2023. https://doi.org/10.1007/978-3-031-32037-8_5

[2] C. Vincent-Lambert, A. Pretorius, and B. Van Tonder, "Use of unmanned aerial vehicles in wilderness search and rescue operations: A scoping review," *Wilderness Environ. Med.*, vol. 34, no. 4, pp. 580–588, 2023. https://doi.org/10.1016/j.wem.2023.08.022

[3] C. Chen, "Development of a multi-parameter measuring device for robots using positioning environment perception," in *Proc. 2021 IEEE 5th Inf. Technol., Netw., Electron. Autom. Control Conf. (ITNEC)*, 2021, vol. 50, pp. 38–41. https://doi.org/10.1109/ITNEC52019.2021.9587156

[4] H.-Y. Lin and J.-R. Zhan, "GNSS-denied UAV indoor navigation with UWB incorporated visual-inertial odometry," *Measurement*, vol. 206, p. 112256, 2023. https://doi.org/10.1016/j.measurement.2022.112256

[5] R. Wang, D. Becker, and T. Hobiger, "Stochastic modeling with robust Kalman filter for real-time kinematic GPS single-frequency positioning," *GPS Solutions*, vol. 27, no. 3, 2023. https://doi.org/10.1007/s10291-023-01479-5

[6] T. Zhang, C. Liu, J. Li, M. Pang, and M. Wang, "A new visual-inertial simultaneous localization and mapping (SLAM) algorithm based on point and line features," *Drones*, vol. 6, no. 1, p. 23, 2022. https://doi.org/10.3390/drones6010023

[7] F. Khobkhun, M. A. Hollands, J. Richards, and A. Ajjimaporn, "Can we accurately measure axial segment coordination during turning using inertial measurement units (IMUs)?" *Sensors*, vol. 20, no. 9, p. 2518, 2020. https://doi.org/10.3390/s20092518

[8] S. Dian, Y. Yin, C. Wu, Y. Zhong, H. Zhang, and H. Yuan, "Loop closure detection based on local-global similarity measurement strategies," *J. Electron. Imaging*, vol. 31, no. 2, 2022. https://doi.org/10.1117/1.jei.31.2.023004

[9] X. Li, H. Wang, Z. Chen, Z. Jiang, and J. Luo, "UWB-Fi: Pushing Wi-Fi towards ultra-wideband for fine-granularity sensing," in *Proc. 22nd Annu. Int. Conf. Mobile Syst., Appl. Services*, 2024. https://doi.org/10.1145/3643832.3661889

[10] M. Gupta and S. Varma, "Metaheuristic-based optimal 3D positioning of UAVs forming aerial mesh network to provide emergency communication services," *IET Commun.*, vol. 15, no. 10, pp. 1297–1314, 2021. https://doi.org/10.1049/cmu2.12112

[11] Y. Zhou, X. Li, S. Li, X. Wang, and Z. Shen, "Ground-VIO: Monocular visual-inertial odometry with online calibration of camera-ground geometric parameters," *IEEE Trans. Intell. Transp. Syst.*, vol. 25, no. 10, pp. 14328–14343, 2024. https://doi.org/10.1109/tits.2024.3393125

[12] M. Jun, Z. Lilian, H. Xiaofeng, Q. Hao, and H. Xiaoping, "A 2D georeferenced map-aided visual-inertial system for precise UAV localization," in *Proc. 2022 IEEE/RSJ Int. Conf. Intell. Robots Syst. (IROS)*, 2022. https://doi.org/10.1109/IROS47612.2022.9982254

[13] W. Guan, P. Chen, Y. Xie, and P. Lu, "PL-EVIO: Robust monocular event-based visual-inertial odometry with point and line features," *IEEE Trans. Autom. Sci. Eng.*, vol. 21, no. 4, pp. 6277–6293, 2024. https://doi.org/10.1109/tase.2023.3324365

[14] U. V. B. L. Udugama, G. Vosselman, and F. Nex, "Mono-Hydra: Real-time 3D scene graph construction from monocular camera input with IMU," *ISPRS Ann. Photogramm., Remote Sens. Spatial Inf. Sci.*, vol. X-1/W1-2023, pp. 439–445, 2023. https://doi.org/10.5194/isprs-annals-x-1-w1-2023-439-2023

[15] M.-M. Gurgu, J. P. Queralta, and T. Westerlund, "Vision-based GNSS-free localization for UAVs in the wild," in *Proc. 2022 7th Int. Conf. Mech. Eng. Robot. Res. (ICMERR)*, 2022. https://doi.org/10.1109/ICMERR56497.2022.10097798

[16] J. Bednar, M. Petrlik, K. C. T. Vivaldini, and M. Saska, "Deployment of reliable visual-inertial odometry approaches for unmanned aerial vehicles in real-world environment," in *Proc. 2022 Int. Conf. Unmanned Aircraft Syst. (ICUAS)*, 2022. https://doi.org/10.1109/ICUAS54217.2022.9836067

[17] B. Gao, B. Lian, and C. Tang, "Semi-direct point-line visual-inertial odometry for MAVs," *Appl. Sci.*, vol. 12, no. 18, p. 9265, 2022. https://doi.org/10.3390/app12189265

[18] R. Tian, Y. Zhang, D. Zhu, S. Liang, S. Coleman, and D. Kerr, "Accurate and robust scale recovery for monocular visual odometry based on plane geometry," in *Proc. 2021 IEEE Int. Conf. Robot. Autom. (ICRA)*, 2021. https://doi.org/10.1109/icra48506.2021.9561215

[19] S. Zhao, H. Zhang, P. Wang, L. Nogueira, and S. Scherer, "Super odometry: IMU-centric LiDAR-visual-inertial estimator for challenging environments," in *Proc. 2021 IEEE/RSJ Int. Conf. Intell. Robots Syst. (IROS)*, 2021. https://doi.org/10.1109/iros51168.2021.9635862

[20] J. Ross, O. Mendez, A. Saha, M. Johnson, and R. Bowden, "BEV-SLAM: Building a globally-consistent world map using monocular vision," in *Proc. 2022 IEEE/RSJ Int. Conf. Intell. Robots Syst. (IROS)*, 2022. https://doi.org/10.1109/IROS47612.2022.9981258

[21] P. Mathur, Y. Jangir, and N. Goveas, "A generalized Kalman filter augmented deep-learning-based approach for autonomous landing in MAVs," in *Proc. 2021 Int. Symp. Asian Control Assoc. Intell. Robot. Ind. Autom. (IRIA)*, 2021, vol. 34, pp. 1–6. https://doi.org/10.1109/iria53009.2021.9588758

[22] C. Hao, X. Jingao, L. Danyang, Z. Yang, and L. Yunhao, "EventBoost: Event-based acceleration platform for real-time drone localization and tracking," in *Proc. IEEE INFOCOM*, 2024, vol. 3, pp. 1851–1859. https://doi.org/10.1109/IFCOM52122.2024.10621101

[23] J. Kühne, M. Magno, and L. Benini, "Low latency visual-inertial odometry with on-sensor accelerated optical flow for resource-constrained UAVs," *IEEE Sens. J.*, pp. 1–1, 2024. https://doi.org/10.1109/JSEN.2024.3406948

[24] M. Miraki and H. Sohrabi, "Using canopy height model derived from UAV imagery as an auxiliary for spectral data to estimate the canopy cover of mixed broadleaf forests," *Environ. Monit. Assess.*, vol. 194, no. 1, 2021. https://doi.org/10.1007/s10661-021-09695-7

[25] Q. Liu, C. Gao, R. Shang, Z. Peng, R. Zhang, and L. Gan, "Environment perception-based seamless indoor and outdoor positioning system of a smartphone," *IEEE Sensors J.*, vol. 22, no. 17, pp. 17205–17215, 2022. https://doi.org/10.1109/jsen.2022.3192911

[26] M. M. Raja, M. H. Arshad, X. Zhang, and Q. Zhao, "Linear quadratic Gaussian control for UAVs with improved state estimation against gyroscope and accelerometer biases," *IFAC-PapersOnLine*, vol. 56, no. 2, pp. 3132–3137, 2023. https://doi.org/10.1016/j.ifacol.2023.10.14

[27] T. Bouazza, T. Hamel, and C. Samson, "Observer design for visual-inertial estimation of pose, linear velocity, and gravity direction in planar environments," *Eur. J. Control*, vol. 80, p. 101067, Nov. 2024. https://doi.org/10.1016/j.ejcon.2024.101067

[28] C. Pan et al., "Tightly coupled integration of monocular visual-inertial odometry and UC-PPP based on factor graph optimization in difficult urban environments," *GPS Solut.*, vol. 28, no. 1, 2023. https://doi.org/10.1007/s10291-023-01586-3

[29] P. Suanpang and P. Jamjuntr, "Optimizing autonomous UAV navigation with D* algorithm for sustainable development," *Sustainability*, vol. 16, no. 17, p. 7867, Sep. 2024. https://doi.org/10.3390/su16177867

[30] X. Fang, Q. Li, Q. Li, K. Ding, and J. Zhu, "Exploiting graph and geodesic distance constraint for deep learning-based visual odometry," *Remote Sens.*, vol. 14, no. 8, p. 1854, 2022. https://doi.org/10.3390/rs14081854

[31] W. Xu, D. Yang, J. Liu, Y. Li, and M. Zhou, "A visual navigation algorithm for UAV based on visual-geography optimization," *Drones*, vol. 8, no. 7, p. 313, Jul. 2024. https://doi.org/10.3390/drones8070313